Phase diagram of chiral 2-flavor QCD based on an effective approach

Edgar López-Contreras, José Antonio García-Hernández, Elías Natanael Polanco-Euán, Wolfgang Bietenholz

Instituto de Ciencias Nucleares Universidad Nacional Autónoma de México A.P. 70-543, C.P. 04510 Ciudad de México, Mexico

Despite intense experimental and theoretical research, the QCD phase diagram at finite baryon density remains to a large extent unexplored. From the theoretical side, the obvious non-perturbative approach is lattice QCD simulations, which are, however, obstructed by a severe sign problem. Here we employ the O(4) non-linear σ -model as an effective theory for 2-flavor QCD in the chiral limit. The identical pattern of spontaneous symmetry breaking indicates that they belong to the same universality class. We assume high temperature dimensional reduction to the 3d O(4) model, with topological charge taking the role of the baryon number, along the lines of Skyrme's model. In this effective formulation, the baryonic chemical potential μ_B can be included in the lattice formulation without causing any sign problem in Monte Carlo simulations. This allows us to pin down the critical line, *i.e.* the critical temperature $T_c(\mu_B)$, which decreases monotonically for increasing μ_B . In the range $0 < \mu_B \lesssim 309$ MeV and 132 MeV $\gtrsim T_c \gtrsim 106$ MeV, we do not find a Critical Endpoint (CEP), although there are hints for it to be in the vicinity of the maximal μ_B -value that we could explore.

Contents

1	The	e mysterious QCD phase diagram	2			
2	The QC	e $\mathrm{O}(4)$ model as an effective theory for chiral 2-flavor D	4			
3	Lattice formulation and simulation					
	3.1	Lattice action	6			
	3.2	Topological charge	7			
		Simulation				
4	Critical line and search for a Critical Endpoint					
	4.1	Numerical results	13			
	4.2	Thermodynamic extrapolation	19			
		Conversion to physical units				
5	Cor	nclusions and outlook	22			

1 The mysterious QCD phase diagram

While a large part of the particle physics community discusses (or speculates) about physics beyond the Standard Model, there are still interesting open questions within the Standard Model. A particularly outstanding issue is the *QCD phase diagram*.

At considerable baryon density, which is especially relevant for neutron stars and for the early Universe, this phase diagram is still a matter of speculations. It is widely assumed — though not certain — that the cross-over between the confined and deconfined phase at low baryon density, which corresponds to a small baryonic chemical potential $\mu_{\rm B}$, ends in a Critical Endpoint (CEP). A number of laboratories are performing experimental searches for this CEP, or are planning to do so: this includes the Relativistic Heavy Ion Collider (RHIC), SPS and all major LHC experiments at CERN, the Nuclotron-based Ion Collider facility (NICA) in Dubna, the Facility for Antiproton and Ion Research (FAIR) in Darmstadt, the Japan Proton Accelerator Research Complex (J-PARC) and the Heavy Ion Research Facility (HIRFL) in Lanzhou.

At $\mu_{\rm B}=0$, the pseudocritical temperature $T_{\rm pc}$ has been successfully measured in lattice QCD simulations. This is the obvious method to be applied, since the issue is clearly non-perturbative. Due to the nature of the cross-over, the value of $T_{\rm pc}$ that one obtains depends somewhat on the criterion that one refers to. There is a consensus that $T_{\rm pc}\approx 155\,{\rm MeV}$ is a sensible value [1].

In the theoretical framework, we can also study the scenario of vanishing masses of the light quark flavors, $m_u = m_d = 0$. In many respects, this is a good approximation to reality, e.g. the nucleon mass is just reduced at percent-level [2]. In the chiral limit, the cross-over turns into a second order phase transition [3], and the critical temperature at $\mu_{\rm B} = 0$ was obtained at $T_{\rm c} \simeq 132\,{\rm MeV}$ [4] with the s-quark at its physical mass, and similarly at $T_{\rm c} \simeq 134\,{\rm MeV}$ when even the c-quark is included [5]. We take the former value as our reference for the $T_{\rm c}$. An alternative study in Ref. [6] actually simulated chiral 2-flavor QCD, with staggered fermions and an irrelevant 4-fermion term, though with less stringent results for the critical temperature.

In this work, we are going to refer to chiral 2-flavor QCD. In this theory, the second-order phase transition line (which is free of ambiguities) is again expected to end in a CEP, where the phase transition turns into first order. In the region of even larger $\mu_{\rm B}$, one may speculate about a variety of new phases, as in the case of physical quark masses.

The reason why the extension of the QCD phase diagram to finite $\mu_{\rm B}$ has not yet been explored by lattice simulations is that they are confronted with a severe sign problem. The Euclidean action becomes complex, hence it cannot be used to directly define a probability density for the importance sampling of the gauge configurations. In principle, the imaginary part can be treated by re-weighting. However, for that approach to provide results with reasonably small errors, tremendous statistics are necessary — the statistical requirement grows exponentially with the volume.

Attempts to overcome this sign problem are reviewed for instance in Refs. [7]. They include simulations with a complex Langevin algorithm (where, however, the compact link variables leave the gauge group SU(3)), simulations at imaginary $\mu_{\rm B}$ (one then tries to extrapolate $\mu_{\rm B}^2$ from negative to positive values), or the numerical computation of Taylor series coefficients at $\mu_{\rm B}=0$ as another basis for an extrapolation to $\mu_{\rm B}>0$.

So far no breakthrough has been achieved with such approaches, hence for the time being it is fully legitimate to employ effective models for this study. A number of such models have been investigated already, such as the Nambu-Jona-Lasinio [8] and Polyakov-Nambu-Jona-Lasinio model [9], the linear σ -model [10], as well as a holographic image approach [11].

In this work, our effective theory is the O(4) non-linear σ -model, in the spirit of Skyrme's model [12]. The concept simplifies if we assume dimensional reduction to the 3d O(4), as we are going to discuss in Section 2. We anticipate that the emerging topological charge Q corresponds to the baryon number B, and that this formulation enables lattice simulations at baryonic chemical potential $\mu_B > 0$ without any sign problem. Preliminary results of this work have been presented in a thesis [13] and in two proceedings contributions [14].

Section 2 motivates our effective theory, and Section 3 explains the lattice formulation that we use, in particular regarding the topological charge. Section 4 presents our numerical results, which are further discussed — and compared to other conjectures in the literature — in Section 5.

The O(4) model as an effective theory for chiral 2-flavor QCD

In Nature, two quark flavors are two orders of magnitude lighter than the intrinsic scale of QCD, m_u , $m_d \ll \Lambda_{\rm QCD}$, hence the chiral limit $m_u = m_d = 0$ is often a good approximation, as we mentioned before. In this limit, the left- and right-handed quarks of 2-flavor QCD decouple, and the Lagrangian has a global $U(2)_L \otimes U(2)_R$ symmetry, where the subscripts denote the quark chiralities. If we separate the two U(1) phase factors (one of them accounts for baryon number conservation and the other one breaks explicitly under quantization due to the axial anomaly), we observe — at low energy — the spontaneous breaking of chiral flavor symmetry as follows,

$$\mathrm{SU}(2)_L \otimes \mathrm{SU}(2)_R \ o \ \mathrm{SU}(2)_{L=R} \ .$$

Adding quark masses turns the three emerging Nambu-Goldstone bosons into the massive pion triplet, but here we stay in the massless case.

The low-energy effective theory is formulated in terms of the Nambu-Goldstone bosons, with a Lagrangian that is invariant under the unbroken symmetry group. We represent the Nambu-Goldstone field by the classical spin $\vec{e}(x) \in S^3$ (i.e. $\vec{e}(x) \in \mathbb{R}^4$ and $|\vec{e}(x)| = 1$, $\forall x$). We restrict the effective

Lagrangian in continuous Euclidean space to the leading term

$$\mathcal{L}_{\text{eff}} = \frac{F_{\pi}^2}{2} \, \partial_{\mu} \vec{e}(x) \cdot \partial_{\mu} \vec{e}(x) \;, \tag{2.1}$$

which has a global O(4) symmetry. F_{π} is a low-energy constant, namely the pion decay constant, which has the phenomenological value $F_{\pi} \simeq 92.4$ MeV. We do not include higher-derivative terms, nor an explicit symmetry-breaking term $-\vec{h} \cdot \vec{e}(x)$, where the norm of the (constant) external "magnetic field", $|\vec{h}|$, would give rise to a degenerate quark mass, $m_u = m_d$.

In its absence (and in infinite volume), the symmetry breaking $O(4) \rightarrow O(3)$ is spontaneous; it can be viewed as a spontaneous "magnetization". Thus we have local isomorphies (which we denote by the symbol $\stackrel{\sim}{-}$) both before and after symmetry breaking,

$$\{ \operatorname{SU}(2)_{L} \otimes \operatorname{SU}(2)_{R} \stackrel{\sim}{\longrightarrow} \operatorname{O}(4) \} \rightarrow \{ \operatorname{SU}(2)_{L=R} \stackrel{\sim}{\longrightarrow} \operatorname{O}(3) \}.$$
 (2.2)

If the O(4) model and chiral 2-flavor QCD are both formulated in 4 dimensions, this relation strongly suggests that their critical points belong to the same universality class. The field $\vec{e}(x) \in S^3 = O(4)/O(3)$ is formulated in the coset space of the symmetry breaking, hence it represents the (massless) pions in the broken phase, according to Chiral Perturbation Theory. The question remains how this mesonic model can address baryons.

Inspired by Skyrme's model [12], but following a somewhat different approach, we assume the temperature T to be high enough for the system to undergo dimensional reduction. This means that the configurations $[\vec{e}]$, which dominate the functional integral, are approximately constant in the Euclidean time direction: its extent β is short, so the periodic boundary conditions suppress the temporal non-zero modes, and the action (in a spatial volume $V = L^3$, $L \gg \beta$) can be approximated as

$$S[\vec{e}] = \int_0^\beta dt_E \int_V d^3x \, \frac{F_\pi^2}{2} \, \partial_\mu \vec{e}(x) \cdot \partial_\mu \vec{e}(x)$$

$$\simeq \beta \int_V d^3x \, \frac{F_\pi^2}{2} \, \partial_i \vec{e}(x) \cdot \partial_i \vec{e}(x) = \beta H[\vec{e}] , \qquad (2.3)$$

where i = 1, 2, 3, and H is the Hamilton function.¹

¹Here, β represents the inverse temperature, $\beta = 1/T$, *i.e.* we refer to units where the Boltzmann constant is 1. In lattice units, we are going to deal with values $\beta_{\text{lat}} \approx 1 \ll L$, see Sections 3 and 4.

The important property is that the 3d O(4) model — with periodic boundary conditions — has topological sectors, due to $\pi_3(S^3) = \mathbb{Z}$, as all (N-1)-dimensional O(N) models. Hence we can assign to each continuous configuration a winding number, or topological charge, $Q[\vec{e}] \in \mathbb{Z}$, so the set of continuous configurations is divided into topological sectors. Thanks to the assumption of dimensional reduction, we do not need Skyrme's "stabilizing term" [12].

Still, we follow Skyrme and other authors [12,15] by identifying the topological charge Q with the baryon number B. This can be justified by considering the corresponding currents, and that is the way how the mesonic model manages to take baryons into account. In this formulation, the baryonic chemical potential μ_B takes the role of an imaginary vacuum angle θ , which leaves the Hamilton function real,

$$H[\vec{e}] = \int_{V} d^{3}x \, \frac{F_{\pi}^{2}}{2} \, \partial_{i}\vec{e}(x) \cdot \partial_{i}\vec{e}(x) - \mu_{B}Q[\vec{e}] \in \mathbb{R} . \qquad (2.4)$$

Thus this model represents chiral 2-flavor QCD at finite baryon density, by a well-motivated effective theory, which can be simulated on the lattice without any sign problem, as we are going to discuss next.

3 Lattice formulation and simulation

3.1 Lattice action

In order to simulate the 3d O(4) model, we need to specify a lattice formulation. We are going to use cubic lattices with volumes $V = L^3$, always with periodic boundary conditions in all directions. We first use lattice units (lattice spacing 1), before finally employing the critical temperature T_c to convert the parameters and results to physical units.

For the Euclidean lattice action S_{lat} , we use the standard regularization,

$$\frac{1}{2} \partial_{i} \vec{e}(x) \cdot \partial_{i} \vec{e}(x) \rightarrow \frac{1}{2} (\vec{e}_{x+\hat{i}} - \vec{e}_{x})^{2} = -\vec{e}_{x} \cdot \vec{e}_{x+\hat{i}} + \text{const.}$$

$$\Rightarrow S_{\text{lat}}[\vec{e}] = -\beta_{\text{lat}} \left(\sum_{\langle xy \rangle} \vec{e}_{x} \cdot \vec{e}_{y} + \mu_{B,\text{lat}} Q[\vec{e}] \right) = \beta_{\text{lat}} H_{\text{lat}}[\vec{e}] , \quad (3.1)$$

where i = 1, 2, 3 is summed over, \hat{i} is the lattice unit vector in *i*-direction, and $\langle xy \rangle$ denotes nearest-neighbor lattice sites.

3.2 Topological charge

The challenge is the definition and computation of the topological charge $Q[\vec{e}]$. All lattice configurations can be continuously deformed into one another, so topological sectors do not exist a priori. Any formulation of $Q[\vec{e}]$ implies some kind of continuum interpolation, which can be ambiguous (in particular for rough configurations).

As a guide-line, we follow the geometric definition advocated by Berg and Lüscher in the 2d O(3) model [16]. The idea is to split the lattice plaquettes into triangles and compute, for each triangle, the solid angle of the spherical triangle (with minimal area) that the three spins at its vertices span on S^2 . If we fix a consistent orientation of all triangles (such that the edges between adjacent triangles contribute in the opposite direction), and attach a sign to the spherical triangle $A_{xyz}[\vec{e}]$ depending on its orientation, their sum — normalized by the area of S^2 — must be an integer. This is a sensible definition of the topological charge Q,

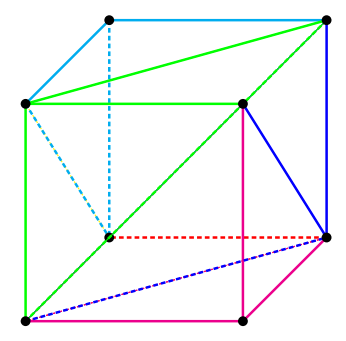
$$Q[\vec{e}] = \frac{1}{4\pi} \sum_{\langle xyz \rangle} A_{xyz}[\vec{e}] \in \mathbb{Z} . \tag{3.2}$$

The sum runs over all index triplets which are vertices of the same triangle. In particular, the property that this definition assigns an integer value to each lattice configuration is a great advantage of the geometric definition compared to other suggestions in the literature. (We can ignore the exceptional cases where the spherical triangle with minimal area $|A_{xyz}|$ is ambiguous, since these configurations form a subset of measure zero.)

In the 3d O(4) model, we follow the same concept, but it becomes more complicated. We decompose each lattice unit cube into six tetrahedra, with an orientation such that the faces between adjacent tetrahedra contribute with opposite planar orientations [17]. A way to do so is depicted in Figure 1 on the left.

The volumes and shapes of these tetrahedra differ, but what matters is that they are space-filling. (A decomposition of the unit cubes into five tetrahedra would also be possible, as depicted in Ref. [18].)²

²In the 2d O(3) model, it is an elegant alternative to use a lattice consisting of regular triangles, which the oriented solid angles A_{xyz} refer to. Hence one might be tempted to suggest for the 3d O(4) model a lattice of regular tetrahedra. This fails, however, since these tetrahedra are not exactly space-filling. The fascinating history of the analysis of space-filling tetrahedra, which began in Ancient Greece, is reviewed in Ref. [18].



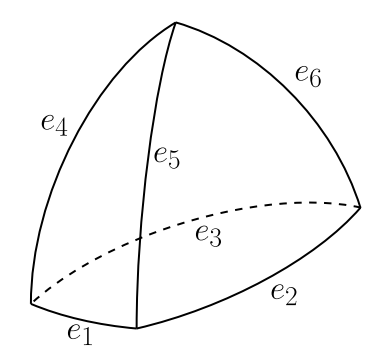


Figure 1: Left: Illustration of the division of a lattice unit cube into six tetrahedra (with distinct colors and line-types), as used in this work. Right: A schematic sketch of a spherical tetrahedron on the sphere S^3 , with edges e_1, \ldots, e_6 .

The four spins at the vertices $\langle wxyz\rangle$ of any tetrahedron span a spherical tetrahedron on S^3 , as symbolically illustrated in the right panel of Figure 1. We again refer to the one with minimal volume, $|V_{wxyz}|$, and attach a sign factor depending on the orientation of this tetrahedron (it corresponds to the sign of the determinant of the matrix $(\vec{e}_w, \vec{e}_x, \vec{e}_y, \vec{e}_z)$). Summing up these oriented volumes, and normalizing by the volume of S^3 , leads to the geometrically defined topological lattice charge

$$Q[\vec{e}] = \frac{1}{2\pi^2} \sum_{\langle wxyz \rangle} V_{wxyz}[\vec{e}] \in \mathbb{Z} , \qquad (3.3)$$

where the sum runs over all lattice site quadruplets that represent vertices of the same tetrahedron.

This conceptual extension of the geometric charge to the 3d O(4) model seems straightforward, but the computation of $V_{wxyz}[\vec{e}]$, *i.e.* of the oriented volume of a spherical tetrahedron, is not. It was only in 2012 that Murakami published a paper with two mathematical recipes (procedures rather than just formulae) for this purpose [19].

The numerical implementation has been successfully achieved by Nava Blanco [20] and also by two of the present authors [13, 21]. The property (3.3) (with an integer to machine precision) for arbitrary configurations is a highly sensitive testing criterion (it fails, for instance, if the orientations are not handled in a fully consistent way).

Moreover, since $Q[\vec{e}]$ represents a winding number, it can also be computed by fixing an arbitrary reference point on S^3 and counting — in an oriented way — how many spherical tetrahedra contain this point. This consistency test was again successful for numerous random configurations, and that method is numerically faster. It does, however, not keep track of the local topological charge density, which is given by $V_{wxyz}[\vec{e}]/(2\pi^2)$.

3.3 Simulation

Our simulations were performed with the multi-cluster algorithm [22, 23], and confirmed by consistency tests with the single-cluster algorithm [23]. Compared to local-update algorithms, the collective cluster flips strongly suppress the critical slowing down near the second order phase transition (see below). The availability of this powerful algorithm is another benefit of the effective theory used in this work.

At $\mu_B = 0$, we follow the standard procedure [23]: we choose a random Wolff direction \vec{r} in 4d spin space, $\vec{r} \in S^3$, and define a "flip" of some spin \vec{e}_x as its reflection at the Wolff hyperplane perpendicular to \vec{r} , $\vec{e}_x \to \vec{e}_x{}' = \vec{e}_x - 2(\vec{r} \cdot \vec{e}_x) \vec{r}$. The energy change under spin flips fixes the probability to set a "bond" between two nearest-neighbor spins. A set of spins connected by bonds constitutes a "cluster". At last, the spins in each cluster are collectively flipped with probability 1/2. Then one chooses a new Wolff direction and repeats the steps above.

At $\mu_B \neq 0$, the bonds are set in the same manner as at $\mu_B = 0$, but the chemical potential alters the cluster-flip probability, which now turns into a Metropolis accept/reject step, based on the term $-\mu_{B,\text{lat}}Q[\vec{e}]$ in $H_{\text{lat}}[\vec{e}]$, see eq. (3.1). This way to include the topological term is analogous to the procedures described in Refs. [24].

Once the chemical potential is turned on, the auto-correlation time increases rapidly, even for the cluster algorithm. The reason is that the clusters are more and more pushed to one side of the Wolff hyperplane. Figure 2 shows the auto-correlation times with respect to the Hamilton function (or energy) τ_H , the magnetization τ_M , and the topological charge, τ_Q , in units of multi-cluster updates (which we denote as "sweeps"). We refer to the exponential auto-correlation time τ obtained by fits of good qualities. We show data for a variety of baryonic chemical potentials $\mu_{B,\text{lat}}$, as functions of the inverse temperature β_{lat} , both in lattice units, in lattice volumes $V = 20^3$.

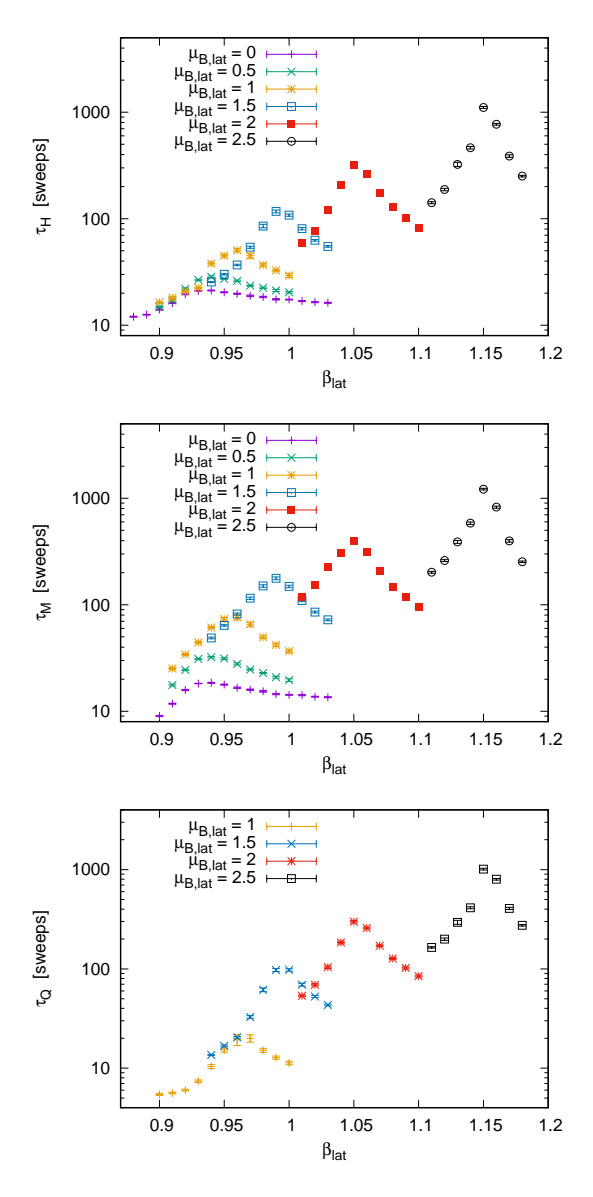


Figure 2: The auto-correlation time with respect to the energy, τ_H (top), the magnetization, τ_M (center), and the topological charge, τ_Q (bottom), all in units of multi-cluster update steps ("sweeps"). We show the exponential auto-correlation time obtained by fits of good qualities, as the small uncertainties confirm. (For $\mu_{B,\text{lat}} < 1$, τ_Q is of $\mathcal{O}(1)$ sweep.) The peak locations provide a first hint for the critical value of β_{lat} , and the peak heights show that the simulations become rapidly more demanding for increasing $\mu_{B,\text{lat}}$.

From Figure 2, we infer the following observations:

- All three auto-correlation times are similar, $\tau_H \approx \tau_M \approx \tau_Q$, which is a great virtue compared to local update algorithms, like Metropolis, Glauber or heatbath, where it is a notorious problem to change the topological sector (except for high temperature), such that τ_Q tends to be huge close to criticality ("topological freezing").
- For $\mu_{B,\text{lat}} \gtrsim 1$, marked peaks show up. They provide a clear hint about the critical temperature. We see that these peaks move to lower temperatures as $\mu_{B,\text{lat}}$ increases, as generally expected in QCD.
- The peak height also increases with $\mu_{B,\text{lat}}$, and at $\mu_{B,\text{lat}} = 2.5$ it attains auto-correlation times of more than 1000 sweeps. We performed all our numerical measurements to be reported in Section 4 such that they were separated by at least $2\tau_{\text{max}}$, where τ_{max} is the longest auto-correlation time for the three observables under consideration. In this manner, the measurements can be considered as independent, and the statistical standard error applies.

This shows that simulations at $\mu_{B,\text{lat}} = 2.5$ are hard. This difficulty prevented us from proceeding to larger values of $\mu_{B,\text{lat}}$ or larger lattice sizes than L = 20. Of course, increasing L does not only have a direct computational cost, but also an indirect one, because τ_{max} again increases rapidly. Still, our results obtained at $L \leq 20$ are conclusive for the critical temperature, as we are going to see.

For completeness, let us also consider the notorious problem of "critical slowing down" in this case. It is quantified by the relation

$$\tau_{\mathcal{O}} \propto \xi^{z_{\mathcal{O}}}$$
, (3.4)

where $\tau_{\mathcal{O}}$ is the autocorrelation time with respect to some observable \mathcal{O} , and ξ is the correlation length (we are going to show results for ξ in Section 4). The proportionality relation refers to the asymptotic behavior as one approaches criticality, and $z_{\mathcal{O}} > 0$ signals the property of critical slowing down, which is worse the larger the maximal value of $z_{\mathcal{O}}$ for the observables of interest. For local-update algorithms, one usually obtains $z_{\mathcal{O}} \approx 2$, which poses a serious problem. Our results (obtained with the cluster algorithm) are shown in Figure 3: at $\mu_{B,\text{lat}} \approx 0$, the slowing down is relatively harmless, but it increases significantly when we proceed to $\mu_{B,\text{lat}} \approx 1$.

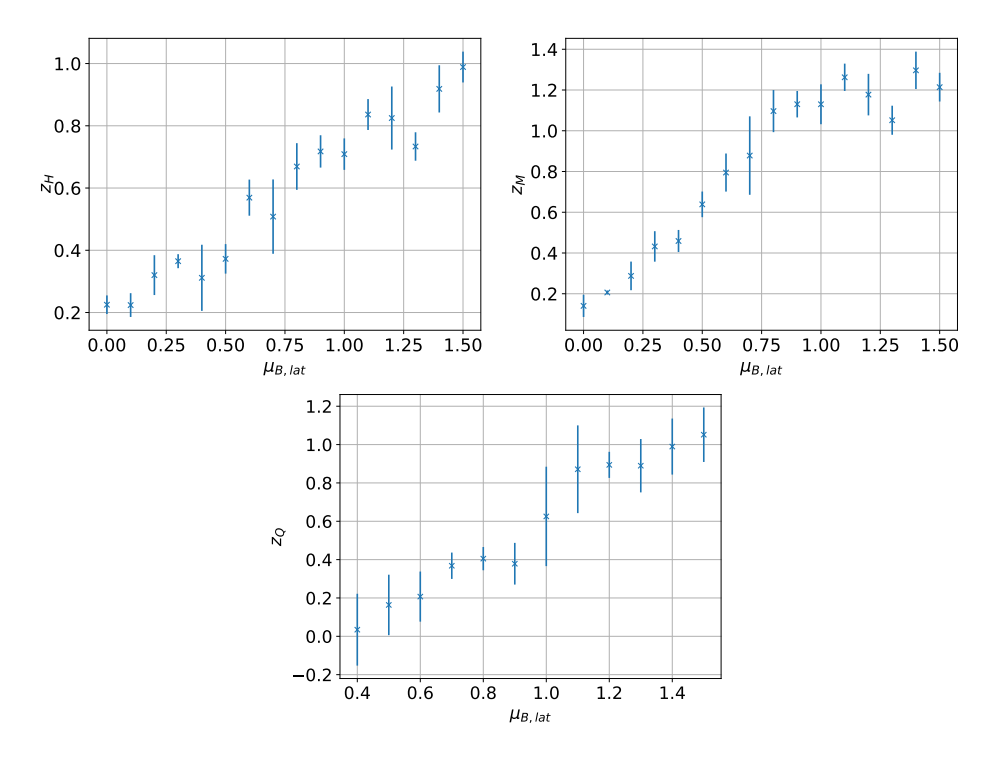


Figure 3: The dynamical critical exponent, based on relation (3.4), with respect to the energy, z_H , the magnetization, z_M , and the topological charge, z_Q . (They are obtained for $\beta_{\rm lat}$ in the vicinity of its critical value, to be discussed in Section 4.) The z-values are very low at $\mu_{B,\rm lat} \approx 0$, which confirms that the critical slowing down is mild in this case, thanks to the cluster algorithm. However, when the baryonic chemical potential increases to $\mu_{B,\rm lat} \approx 1$, the dynamical critical exponents also attain values around 1.

4 Critical line and search for a Critical Endpoint

We repeat that, in the framework of this effective model, a degenerate quark mass corresponds to the strength of an external magnetic field \vec{h} , which gives rise to an additional term $-\vec{h} \cdot \sum_x \vec{e}_x$ in $H_{\text{lat}}[\vec{e}]$. Here we deal with $\vec{h} = \vec{0}$, hence we refer to the chiral limit, where the quark masses and the pion mass vanish. We will, however, occasionally refer also to derivatives with respect to \vec{h} , $\partial_{\vec{h}}$, which are taken at $\vec{h} = \vec{0}$.

We simulate in cubic lattice volumes, L^3 , with L = 10, 12, 16, 20, at

$$\mu_{\text{B,lat}} = 0, 0.1, 0.2, \dots, 1.4, 1.5; 2, 2.5$$
.

At low $\mu_{B,lat}$, we could proceed to larger volumes, but the sharp increase in the auto-correlation time prevents us from doing so at our largest values of $\mu_{B,lat}$, as Figure 2 shows.

4.1 Numerical results

We measure observables, which are given by first or second derivatives of the free energy $F = -(\ln Z)/\beta$. According to Ehrenfest's classification, a discontinuity with respect to β indicates a first or second order phase transition, respectively. At each value of $\mu_{B,lat}$, we have to search for the β -value where a phase transition takes place, $\beta_{c,lat}(\mu_{B,lat})$, and we measure a set of observables in its vicinity.

All our results to be shown below are based on 10^4 configurations for each parameter set. We repeat that they are perfectly decorrelated, *i.e.* measurements are separated at least by $2\tau_{\text{max}}$ sweeps (where τ_{max} is the maximum among τ_H , τ_M , τ_Q), even at the peaks in Figure 2, such that the statistical standard error applies. We first consider a set of results obtained at L=20.

Figure 4 shows three densities, each one given by a first derivative of the free energy F,

energy density :
$$\epsilon = \langle H \rangle / V = -\frac{1}{V} \partial_{\beta}(\beta F)$$
,
magnetization density : $m = \langle |\vec{M}| \rangle / V$, $\vec{M} = \sum_{x} \vec{e_{x}} = \partial_{\vec{h}} F|_{\vec{h}=\vec{0}}$,
topological density : $q = \langle Q \rangle / V$, $\langle Q \rangle = \partial_{\mu_{B}} F$. (4.1)

Note that m is the order parameter. As we increase $\mu_{B,\text{lat}} > 0$, positive topological charge is favored, $\langle Q \rangle > 0$. In fact, the maximum of q indicated in Figure 4 corresponds to an impressive value of $\langle Q \rangle \simeq 665.8$.

The enhancement of the topological windings in the dominant configurations leads to an increase of ϵ , but a decrease of m. This also moves the maximal slope to larger values of β_{lat} , which confirms that the critical temperature decreases as $\mu_{B,\text{lat}}$ grows.

In particular, at $\mu_{B,\text{lat}} = 2.5$ all three densities display a strong slope around $\beta_{\text{lat}} \approx 1.15$. At this point, one might wonder whether it turns into

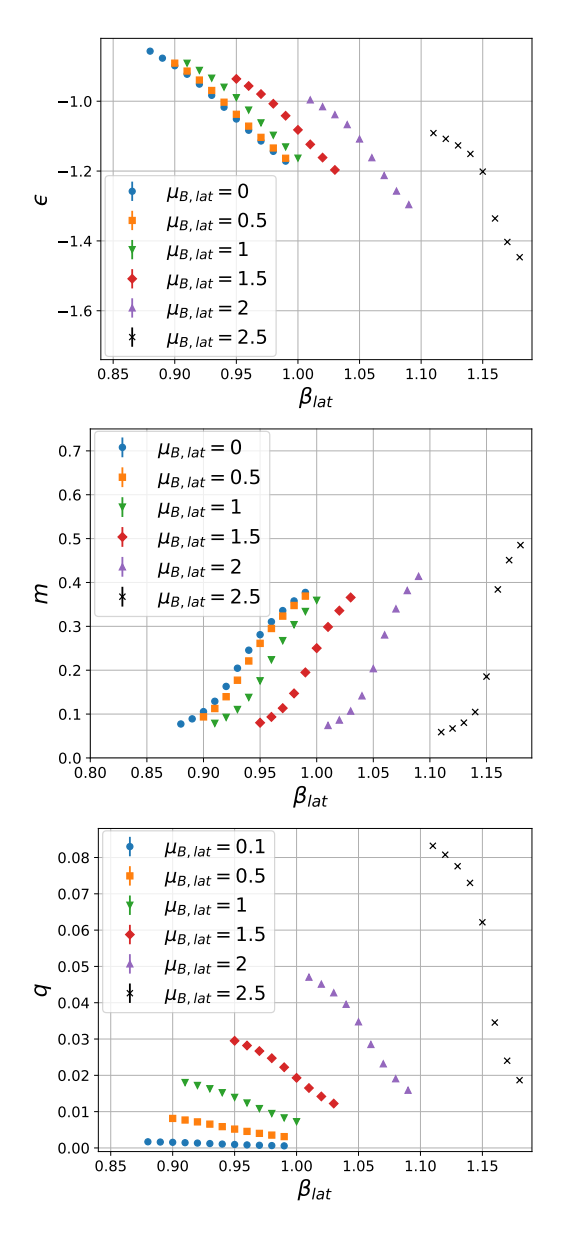


Figure 4: Energy density $\epsilon = \langle H \rangle / V$ (top), magnetization density $m = \langle |\vec{M}| \rangle / V$, $\vec{M} = \sum_x \vec{e_x}$ (center) and topological density $q = \langle Q \rangle / V$ (bottom), for $\mu_{B,\text{lat}} \in [0,2.5]$, in the lattice volume $V = 20^3$. We see that increasing $\mu_{B,\text{lat}}$ moves the interval of maximal slope — which is the vicinity of the phase transition — to larger values of β_{lat} , and this slope becomes steeper. In particular at $\mu_{B,\text{lat}} = 2.5$ one might wonder whether the phase transition is still of second order, or if this would be a jump in infinite volume, *i.e.* a first order phase transition.

a discontinuous jump in infinite volume, *i.e.* whether the first order phase transition is attained already, or if it is at least nearby.

In order to clarify this question, we move on to quantities which are given by second-order derivatives of F: the correlation length ξ (given by the exponential decay of the connected correlation function, which turns into a cosh-behavior in the finite, periodic volume); the specific heat (or heat capacity) c_V ; the magnetic susceptibility $\chi_{\rm m}$; and the topological susceptibility $\chi_{\rm t}$. The latter three quantities are defined as

$$c_{V} = \frac{\beta^{2}}{V} \left(\langle H_{\text{lat}}^{2} \rangle - \langle H_{\text{lat}} \rangle^{2} \right) = \frac{\beta^{2}}{V} \partial_{\beta}^{2} (\beta F) ,$$

$$\chi_{\text{m}} = \frac{\beta}{V} \left(\langle \vec{M}^{2} \rangle - \langle |\vec{M}| \rangle^{2} \right) \stackrel{\wedge}{=} \frac{1}{V} \partial_{\vec{h}}^{2} F ,$$

$$\chi_{\text{t}} = \frac{1}{V} \left(\langle Q^{2} \rangle - \langle Q \rangle^{2} \right) = \frac{1}{V} \partial_{\mu_{B}}^{2} F . \tag{4.2}$$

As long as the phase transition is of second order, we expect for each of these three quantities a peak, which would turn into a divergence at β_c in the thermodynamic limit $V \to \infty$.

Figure 5 shows the correlation length ξ , at L=20. It is measured with a cosh-fit to the correlation function after mapping the configurations on one axis. We also show the second moment correlation length ξ_2 , which is here and in general very similar, but its numerical measurement is easier since no fit is required,

$$\xi_{2} = \sqrt{\frac{\tilde{G}(p=0) - \tilde{G}(2\pi/L, 0, 0)}{4\tilde{G}(2\pi/L, 0, 0) \sin^{2}(\pi/L)}},$$

$$\tilde{G}(p) = \frac{1}{V} \sum_{x} \langle \vec{e_{0}} \cdot \vec{e_{x}} \rangle \exp(-ip \cdot x).$$
(4.3)

The maxima in this plot provide another hint for the values of $\beta_{c,lat}$, consistent with those conjectured from the maximal slopes in Figure 4. However, the apparent divergence of ξ in the thermodynamic limit is evidence for the corresponding phase transition to be of second order.

³In numerical studies of $\chi_{\rm m}$, it is usual to replace $\langle \vec{M} \rangle$ by $\langle |\vec{M}| \rangle$, see *e.g.* Ref. [25], since — strictly speaking — the former always vanishes in the absence of an external magnetic field, even in the broken phase, which prevents us from observing a peak of $\chi_{\rm m}$. The symbol \triangleq (instead of =) keeps track of this modification.

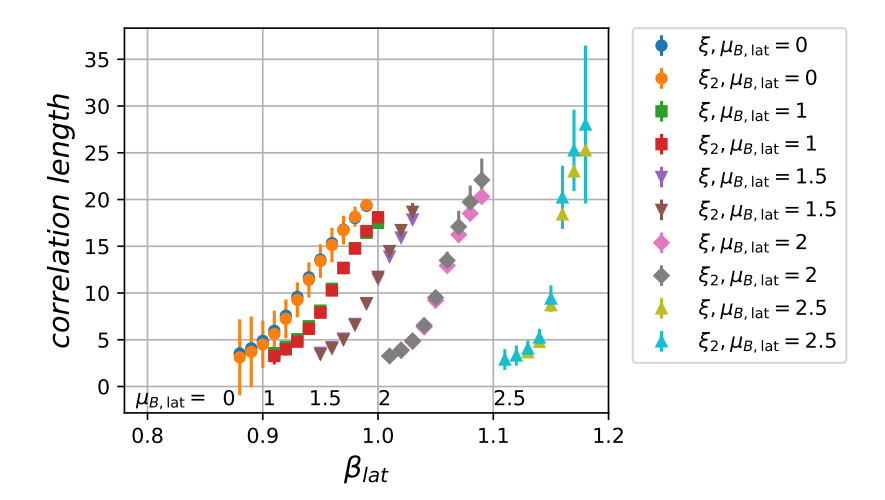


Figure 5: Results for the (standard) correlation length ξ , and for the second moment correlation length ξ_2 , in the volume $V = 20^3$. The hints for a phase transition of Figure 4 are substantiated, now with evidence for the transition to be of second order, and with consistent estimates for $\beta_{\text{c,lat}}(\mu_{B,\text{lat}})$.

We add that the system only behaves similarly to its infinite-volume limit when $\xi \ll L$, which prevents us from obtaining precise results for the critical exponents, see below.

Figure 6 shows results for the specific heat c_V . At L = 20 (upper plot), we see peaks becoming more pronounced as $\mu_{B,\text{lat}}$ increases. This strongly suggests that the phase transition is still of second order up to $\mu_{B,\text{lat}} = 2.5$.

The lower plot compares results for $\mu_{B,\text{lat}} = 1$ (as an example) in four volumes. The data are interpolated by Johnson's S_U ("unbounded system") function J,

$$J(\beta_{\text{lat}}) = \frac{c_1}{\sqrt{1 + ((\beta_{\text{lat}} - c_2)/c_3)^2}} \exp\left(-\left[c_4 + c_5 \sinh^{-1}((\beta_{\text{lat}} - c_2)/c_3)\right]^2\right)$$
(4.4)

with the fitting parameters c_1, \ldots, c_5 . This provides good fits over a sizable range in β_{lat} for all our values of $\mu_{B,\text{lat}}$ (unlike e.g. simple Gaussian fits). We see that the β_{lat} -value, where c_V takes its maximum, β_{max} , moves only marginally with L. That property facilitates the thermodynamic extrapolation to $\beta_{\text{c,lat}}$, which we are going to address in Subsection 4.2.

We also observe that the peak height increases only slightly when the volume is enlarged. Finite-size scaling predicts $c_V(T_c) \propto L^{\alpha/\nu}$, where α

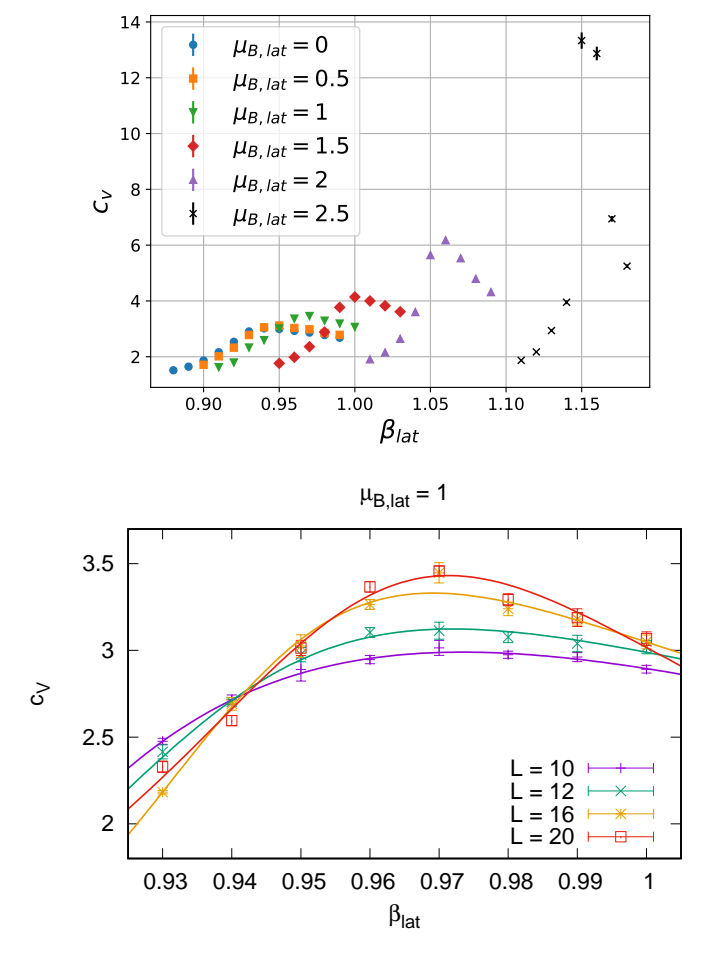


Figure 6: Results for the specific heat c_V . Above: $\mu_{B,\text{lat}} = 0, \dots, 2.5$ in the lattice volume $V = 20^3$. At large $\mu_{B,\text{lat}}$, the peaks are most pronounced: they confirm that the phase transition is still of second order, and they are helpful for the determination of the critical temperature. Below: Finite-size scaling of the peak at $\mu_{B,\text{lat}} = 1$ (as an example), fitted with Johnson's S_U -function, see eq. (4.4): the value of the maximum, β_{max} , hardly moves, and the peak height increases only gradually for larger L.

and ν are the critical exponents in the usual notation. This behavior is consistent with the typically small ratio of these critical exponents: at $\mu_B = 0$, Refs. [26,27] obtained $\nu \simeq 0.75$, such that Josephson's scaling law implies $\alpha/\nu = 3 - 2/\nu \simeq 0.30$. (Unfortunately, the corresponding values that we

extracted at $\mu_B > 0$ [13, 14] are plagued by significant finite-size effects.)

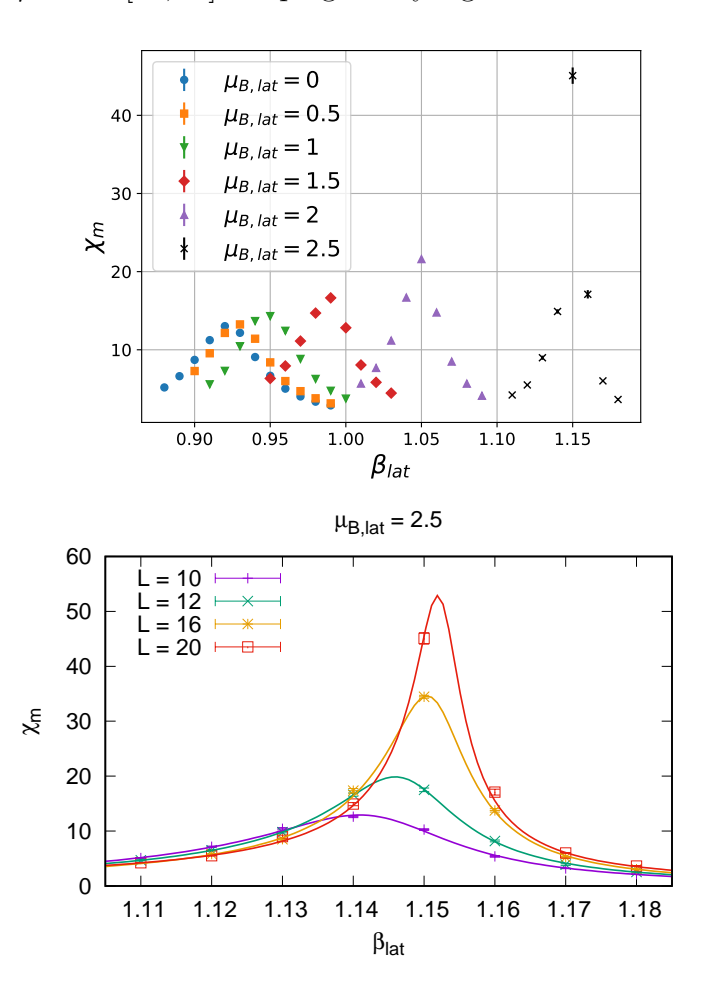


Figure 7: Results for the magnetic susceptibility $\chi_{\rm m}$, in analogy to Figure 6. Above: The peaks in $V=20^3$ provide another way to determine the critical temperature, and to confirm that the phase transition is of second order, for $\mu_{B,\rm lat} \in [0,2.5]$. Below: Data obtained in four volumes, again fitted with Johnson's S_U function of eq. (4.4) in order to identify $\beta_{\rm max}$ by interpolation. Here we show, as an example, the data for $\mu_{B,\rm lat}=2.5$: in this case, we observe a significant volume-dependence of $\beta_{\rm max}$. Moreover, the peak height increases substantially when the volume is enlarged.

For the magnetic susceptibility $\chi_{\rm m}$, defined in eq. (4.2), the results are shown in Figure 7. Here the peak is more visible even down to $\mu_{B,{\rm lat}}=0$.

Again it is most pronounced at $\mu_{B,\text{lat}} = 2.5$, further affirming that the phase transition is of second order all over the range investigated here. In this case, the finite-size effects on β_{max} are stronger than in the case of c_V .

The strongly increasing peak height in enhanced volume is consistent with the finite-size scaling relation $\chi_{\rm m}(T_{\rm c}) \propto L^{\gamma/\nu}$; at $\mu_B=0$, Refs. [26, 27] measured $\gamma/\nu \simeq 1.97$. This value, as well as the one for ν alone, could be determined from simulations in larger volumes, which were accessible due to the much shorter auto-correlation time in the absence of a chemical potential, as shown in Figure 2.

Finally, we proceed to the topological susceptibility χ_t , which is also defined in eq. (4.2). The peaks in Figure 8 assure once more that we are dealing with a second order phase transition for $\mu_{B,\text{lat}} \leq 2.5$.

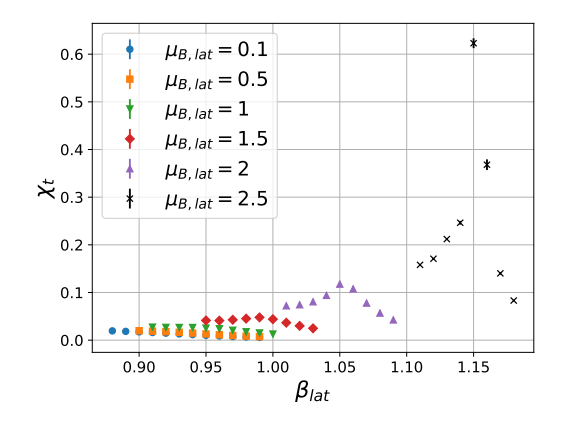
Taking the results for τ_H , τ_M , τ_Q , ξ (and ξ_2), c_V , $\chi_{\rm m}$ and $\chi_{\rm t}$ together provides overwhelming evidence that the critical line extends at least up to $\mu_{B,{\rm lat}} = 2.5$, despite the strong slopes observed in the densities of Figure 4.

4.2 Thermodynamic extrapolation

We have seen indications for the value of the inverse critical temperature $\beta_{c,lat}$ from various perspectives: the peaks of the auto-correlation times in Figure 2 and of the correlation length in Figure 5, the interval of steepest slopes of the densities (as functions of β_{lat}) in Figure 4, and finally the peaks of the quantities in eq. (4.2), which are given by second derivatives of the free energy F. The data for the terms c_V and χ_m are most conclusive for criticality, and we already denoted the β -value where we observe their maxima as β_{max} .

Figure 9 shows the extrapolations of β_{max} to the limit $L \to \infty$ for c_V and χ_{m} , at $\mu_{B,\text{lat}} = 0.1$, 1, and 2.5, as examples. The extrapolated values are not only consistent with the literature at $\mu_{B,\text{lat}} = 0$, but they are also in all cases consistent with each other when deduced from c_V and χ_{m} (within their uncertainties). This shows that — in this regard — the finite-size effects are under control thanks to the extrapolations, although the data are obtained in relatively small volumes. This provides our results for the inverse critical temperature $\beta_{\text{c,lat}}$.

Such extrapolations have been performed at each $\mu_{B,\text{lat}}$ -value in our study, and in all cases we obtained consistent results for $\beta_{c,\text{lat}}(\mu_{B,\text{lat}})$. These critical values are listed in Table 1. They are the basis for the phase diagram, as far as we could explore it.



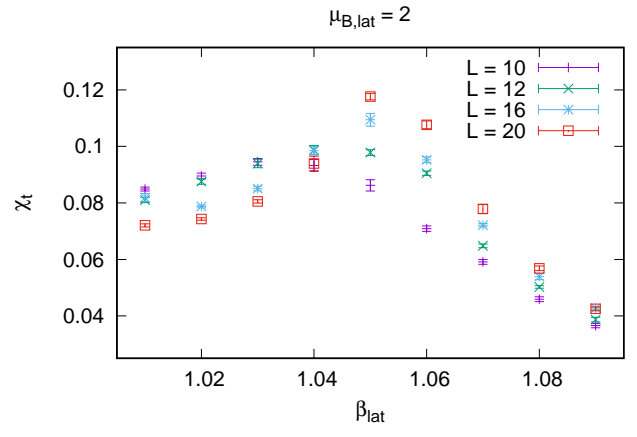


Figure 8: Results for the topological susceptibility χ_t . Above: $\mu_{B,\text{lat}} = 0, \dots, 2.5$ in the lattice volume $V = 20^3$. Below: $\mu_{B,\text{lat}} = 2$ and $V = 10^3$, 12^3 , 16^3 and 20^3 .

4.3 Conversion to physical units

In order to convert the lattice units to physical units, we need a reference quantity, which is known in both units. The obvious choice is the critical temperature $T_{\rm c}=1/\beta_{\rm c}$ at $\mu_B=0$. In the 3d O(4) lattice model it has been computed to high precision by Oevers, who found $\beta_{\rm c,lat}=0.9359(1)$ [28], which is compatible with Ref. [26] and with our result in Table 1. We match this value to the aforementioned critical temperature obtained in chiral QCD, $T_{\rm c}\simeq 132$ MeV [4], cf. Section 1, which leads to

$$\mu_B = \frac{\beta_{\text{c,lat}}}{\beta_{\text{c}}} \mu_{B,\text{lat}} \simeq 124 \text{ MeV } \mu_{B,\text{lat}} .$$
 (4.5)

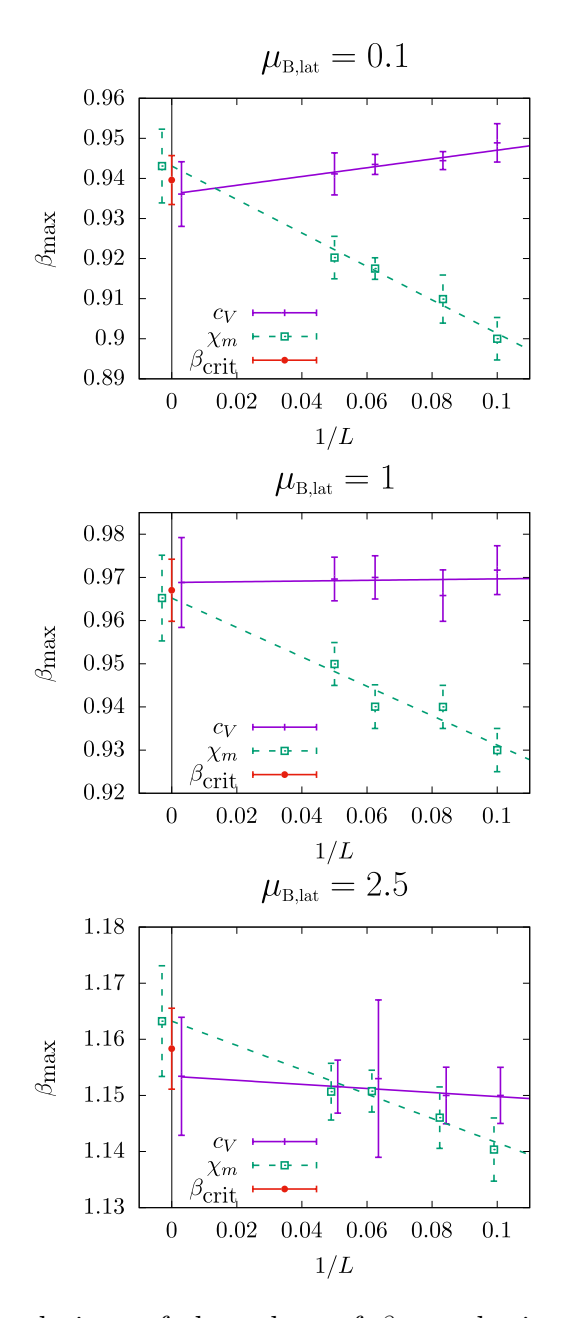


Figure 9: Extrapolations of the values of $\beta_{\rm max}$, obtained by interpolating fits in various volumes, to the critical values in the thermodynamic limit $\beta_{\rm c,lat}$. We show results at $\mu_{B,\rm lat}=0.1,~1,~2.5,$ and we see that in each case the extrapolations based on the specific heat c_V and on the magnetic susceptibility $\chi_{\rm m}$ are consistent.

$\mu_{B,\mathrm{lat}}$	0	0.1	0.2	0.3	0.4	0.5			
$\beta_{\mathrm{c,lat}}$	0.940(5)	0.940(6)	9.943(4)	0.948(7)	0.941(7)	0.951(4)			
$\mu_{B,\mathrm{lat}}$	0.6	0.7	0.8	0.9	1	1.1			
$\beta_{\mathrm{c,lat}}$	0.940(7)	0.948(4)	0.954(5)	0.968(6)	0.967(7)	0.974(5)			
$\mu_{B,\mathrm{lat}}$	1.2	1.3	1.4	1.5	2	2.5			
$\beta_{\mathrm{c,lat}}$	0.986(5)	0.988(8)	1.003(8)	0.997(8)	1.064(11)	1.158(7)			

Table 1: Critical values for the inverse temperature β_{lat} , obtained from extrapolations to infinite volume, at fixed $\mu_{B,lat}$, as illustrated (for three examples) in Figure 9.

Thus we interpret our simulation parameter $\mu_{B,lat} = 0, \dots, 2.5$ as

$$0 \le \mu_B \lesssim 309 \text{ MeV}$$
. (4.6)

By applying the conversion to physical units, we arrive at the phase diagram in Figure 10. This phase diagram summarizes the results of this work, which we are going to discuss in Section 5.

5 Conclusions and outlook

Our point of departure was that the 4d O(4) model is most likely in the universality class of 2-flavor QCD in the chiral limit, along the lines of Skyrme's theory [12]. Unfortunately, O(N) models cannot cope with more than two quark flavors, since the pattern of spontaneous symmetry breaking $O(N) \to O(N-1)$ is not isomorphic to $SU(N_f) \otimes SU(N_f) \to SU(N_f)$ for any $N_f > 2$ [29].

Next we assumed the temperature to be high enough for a dimensional reduction to be a sensible approximation. This leads to the 3d O(4) model, where the configurations carry topological charge Q, which can be identified with the baryon number B. Hence, the baryon chemical potential μ_B takes the form of an imaginary θ -vacuum angle. This term does not cause any sign problem in Monte Carlo simulations.

We simulated this model with a cluster algorithm and monitored the critical line in the range of $\mu_{B,\text{lat}} = 0, \dots, 2.5$ (in lattice units). In physical units, the maximal value is estimated as $\mu_B \simeq 309$ MeV.

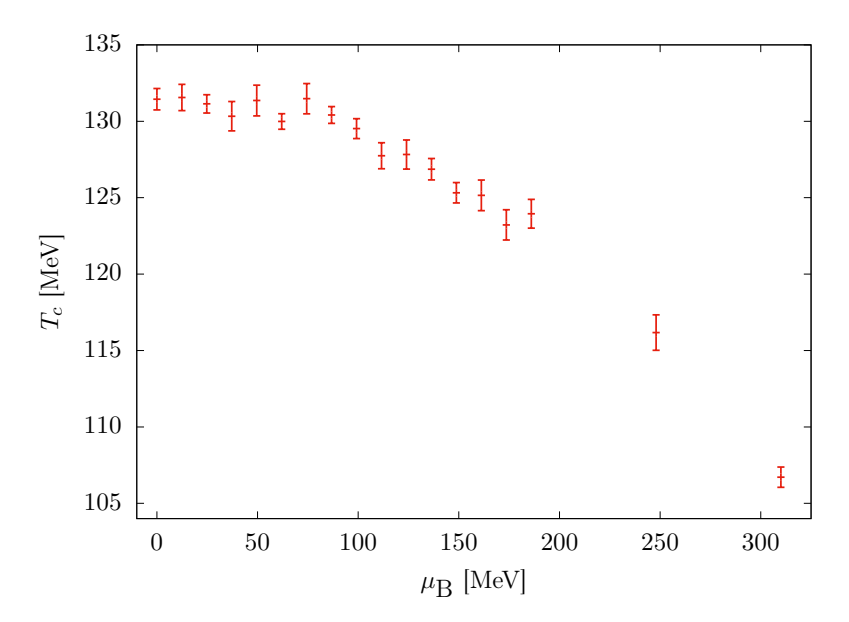


Figure 10: The phase diagram for chiral 2-flavor QCD, based on the 3d O(4) model as an effective theory: our results lead to a critical line from $T_c(0) \simeq 132$ MeV down to $T_c(306 \text{ MeV}) \simeq 106$ MeV.

The critical temperature $T_{\rm c}(\mu_B)$ decreases monotonically, see Figure 10, in agreement with the generally expected behavior in QCD. In our study, it moves from $T_{\rm c}(0) \simeq 132$ MeV down to $T_{\rm c}(309$ MeV) $\simeq 106$ MeV. In this range, we consistently observed a second order phase transition, but in Figure 4 there are hints for the final point to be near a crossing to a first order phase transition.

If we trust this effective theory, then our results imply bounds on the location of a (possible) Critical Endpoint: $T_{\text{CEP}} < 106 \text{ MeV}$, $\mu_{B,\text{CEP}} > 309 \text{ MeV}$, which agrees with part of the predictions in the literature. An overview over such predictions is given in Figure 11, and the corresponding bibliography is collected in Ref. [30]. Part of this list is adopted from Ref. [31].

The inclusion of quark masses corresponds — in our effective theory — to the addition of a constant, external magnetic field. In this modified model, we observe a cross-over rather than a phase transition [14,21]. This alleviates the problem with the very long auto-correlation times in the current study (cf. Subsection 3.3), and the systematic errors due to finite-size effects (cf. Subsection 4.1), since neither the autocorrelation time nor the correlation

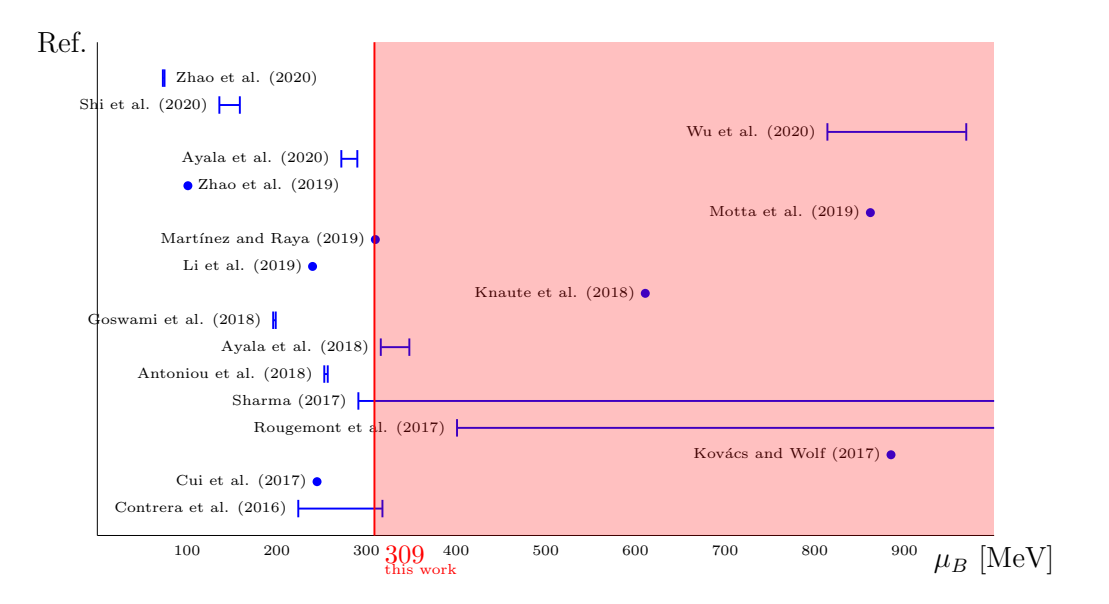
length diverge at the cross-over. On the other hand, the pseudo-critical value $\beta_{\rm pc}$ is somewhat ambiguous, depending on the criterion that one considers. This scenario is under investigation [32]; preliminary results do again not reveal a Critical Endpoint up to $\mu_B \simeq 250$ MeV [14,21].

We are convinced that our phase diagram in Figure 10 provides a noteworthy orientation: the shape of the critical line is compatible with the literature, and it allows us to conjecture bounds for the CEP.

Acknowledgments: We are indebted to Uwe-Jens Wiese for inspiring this project. We also thank Arturo Fernández Téllez and Miguel Ángel Nava Blanco for their contributions at an early stage, Alexis Aguilar-Arevalo for advice with the data analysis, and Victor Muñoz-Vitelly for reading the manuscript. The simulations were performed on the cluster of the Instituto de Ciencias Nucleares; we thank Luciano Díaz González and Eduardo Murrieta León for technical assistance. This project was supported by UNAM-DGAPA through the PAPIIT projects IG100219, "Exploración teórica y experimental del diagrama de fase de la cromodinámica cuántica" and IG100322, "Materia fuertemente acoplada en condiciones extremas con el MPD-NICA", and by the Consejo Nacional de Humanidades, Ciencia y Tecnología (CONAHCYT), which has now been converted into the Secretaría de Ciencia, Humanidades, Tecnología e Innovación (SECIHTI).

References

- [1] S. Borsányi, Z. Fodor, C. Hoelbling, S. D. Katz, S. Krieg, C. Ratti, K. K. Szabó, Is there still any T_c mystery in lattice QCD? Results with physical masses in the continuum limit III, JHEP 1009 (2010) 073. T. Bhattacharya et al. (HotQCD Collaboration), QCD Phase Transition with Chiral Quarks and Physical Quark Masses, Phys. Rev. Lett. 113 (2014) 082001. A. Bazavov et al. (HotQCD Collaboration), Chiral crossover in QCD at zero and non-zero chemical potentials, Phys. Lett. B 795 (2019) 15.
- [2] S. Dürr *et al.*, Lattice computation of the nucleon scalar quark contents at the physical point, *Phys. Rev. Lett.* **116** (2016) 172001.
- [3] R.D. Pisarski and F. Wilczek, Remarks on the chiral phase transition in chromodynamics, *Phys. Rev. D* **29** (1984) 338. F. Wilczek, Application



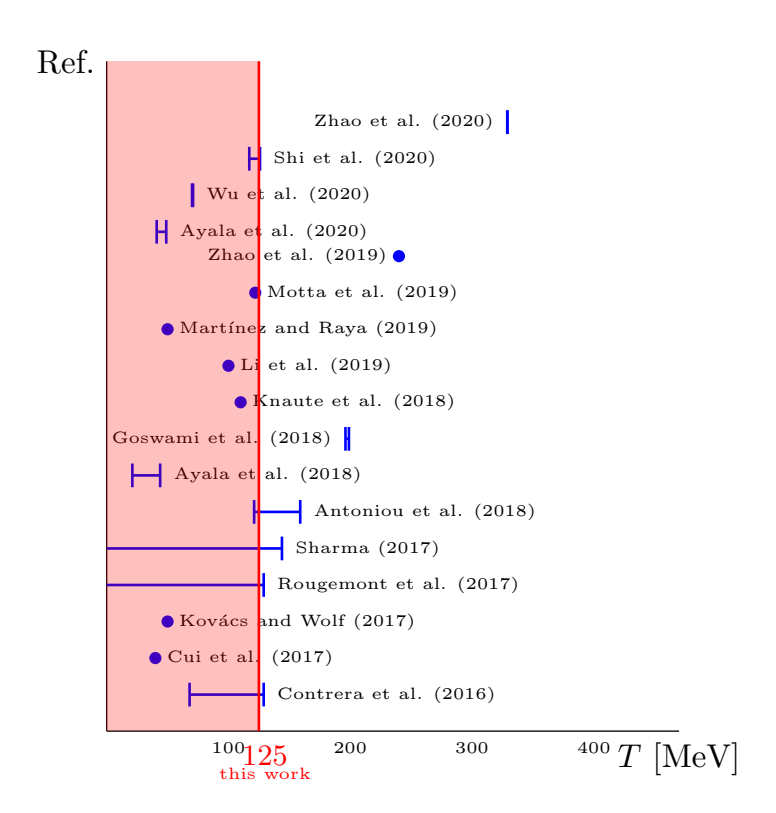


Figure 11: Overview of estimates for the location of the CEP in the (μ_B, T) plane. The conjectures in 17 papers — based on a broad variety of assumptions and techniques — are compared to the outcome of this work.

- of the renormalization group to a second order QCD phase transition, Int. J. Mod. Phys. A 7 (1992) 3911 [Erratum: Int. J. Mod. Phys. A 7 (1992) 6951]. K. Rajagopal and F. Wilczek, Static and dynamic critical phenomena at a second order QCD phase transition, Nucl. Phys. B 399 (1993) 395. S. Ejiri, R. Iwami and N. Yamada, Exploring the nature of chiral phase transition in two-flavor QCD using extra heavy quarks, Phys. Rev. D 93 (2016) 054506. A. Yu. Kotov, M. P. Lombardo and A. Trunin, Gliding Down the QCD Transition Line, from $N_{\rm f}=2$ till the Onset of Conformality, Symmetry 13 (2021) 1833.
- [4] H.-T. Ding et al. (HotQCD Collaboration), Chiral phase transition temperature in (2+1)-Flavor QCD, Phys. Rev. Lett. 123 (2019) 062002.
- [5] A.Yu. Kotov, M.P. Lombardo and A. Trunin, QCD transition at the physical point, and its scaling window from twisted mass Wilson fermions, *Phys. Lett. B* **823** (2021) 136749.
- [6] J.B. Kogut and D.K. Sinclair, Evidence for O(2) universality at the finite temperature transition for lattice QCD with 2 flavors of massless staggered quarks, *Phys. Rev.* D **73** (2006) 074512.
- [7] P. de Forcrand, Simulating QCD at finite density, *PoS LAT2009 (2009) 010*. L. Levkova, QCD at nonzero temperature and density, *PoS LAT-TICE2011 (2011) 011*. C. Ratti, Lattice QCD and heavy ion collisions: a review of recent progress, *Rept. Prog. Phys.* 81 (2018) 084301.
- [8] Z.F. Cui, J.L. Zhang and H.S. Zong, Proper time regularization and the QCD chiral phase transition, Sci. Rep. 7 (2017) 45937. J. Braun, M. Leonhardt and M. Pospiech, Fierz-complete NJL model study III: Emergence from quark-gluon dynamics, Phys. Rev. D 101 (2020) 036004.
- [9] G.A. Contrera, A.G. Grunfeld and D. Blaschke, Supporting the search for the CEP location with nonlocal PNJL models constrained by lattice QCD, Eur. Phys. J. A 52 (2016) 231. Y.P. Zhao, S.Y. Zuo and C.M. Li, QCD phase diagram and critical exponents within the nonextensive Polyakov-Nambu-Jona-Lasinio model, Chin. Phys. C 45 (2021) 073105.
- [10] A. Ayala, S. Hernández-Ortiz, L.A. Hernández, V. Knapp-Pérez and R. Zamora, Fluctuating temperature and baryon chemical potential in heavy-ion collisions and the position of the critical end point in the

- effective QCD phase diagram, *Phys. Rev. D* **101** (2020) 074023. A. Ayala, B. Almeida Zamora, J.J. Cobos-Martínez, S. Hernández-Ortiz, L.A. Hernández, A. Raya and M.E. Tejeda-Yeomans, Collision energy dependence of the critical end point from baryon number fluctuations in the Linear Sigma Model with quarks, *Eur. Phys. J. A* **58** (2022) 87.
- [11] O. DeWolfe, S.S. Gubser and C. Rosen, Dynamic critical phenomena at a holographic critical point, *Phys. Rev. D* 84 (2011) 126014. R. Critelli, J. Noronha, J. Noronha-Hostler, I. Portillo and C. Ratti, Critical point in the phase diagram of primordial quark-gluon matter from black hole physics, *Phys. Rev. D* 96 (2017) 096026. Z. Li, K. Xu and M. Huang, The entanglement properties of holographic QCD model with a critical end point, *Chin. Phys. C* 45 (2021) 013116.
- [12] T.H.R. Skyrme, A Nonlinear field theory, Proc. Roy. Soc. Lond. A 260 (1961) 127; A unified field theory of mesons and baryons, Nucl. Phys. 31 (1962) 556.
- [13] E. López-Contreras, Phase Diagram of the 3d O(4) model as a conjecture for Quantum Chromodynamics in the chiral limit, B.Sc. thesis, Universidad Nacional Autónoma de México, 2021.
- [14] J.A. García-Hernández, E. López-Contreras, E.N. Polanco-Euán and W. Bietenholz, Conjecture about the QCD phase diagram, *PoS LAT2021* (2021) 595. E. López-Contreras, J.A. García-Hernández, E.N. Polanco-Euán and W. Bietenholz, The 3d O(4) model as an effective approach to the QCD phase diagram, *Rev. Mex. Fis. Suppl.* 3 (2022) 020727.
- [15] G.S. Adkins, C.R. Nappi and E. Witten, Static properties of nucleons in the Skyrme model, *Nucl. Phys. B* 228 (1983) 552. I. Zahed and G.E. Brown, The Skyrme Model, *Phys. Rept.* 142 (1986) 1.
- [16] B. Berg and M. Lüscher, Definition and Statistical Distributions of a Topological Number in the Lattice O(3) Sigma Model, *Nucl. Phys. B* 190 (1981) 412.
- [17] U.-J. Wiese, Topologie von (Gitter-)Eichfeldern, Ph.D. thesis, Universität Hannover, 1986.
- [18] M. Senechal, Which Tetrahedra Fill Space?, Mathematics Magazine 54 (1981) 227.

- [19] J. Murakami, Volume formulas for a spherical tetrahedron, *Proc. Amer. Math. Soc.* **140** (2012) 3289.
- [20] M. A. Nava Blanco, W. Bietenholz and A. Fernández Téllez, Conjecture about the 2-Flavour QCD Phase Diagram, J. Phys. Conf. Ser. 912 (2017) 012048. M. A. Nava Blanco, Estudio del diagrama de fase de QCD con dos sabores usando el modelo 3d O(4), M.Sc. thesis, Benemérita Universidad Autónoma de Puebla, 2019.
- [21] J.A. García-Hernández, Conjecture about the Quantum Chromodynamics Phase Diagram with two Light Quark Flavors, B.Sc. thesis, Universidad Nacional Autónoma de México, 2020.
- [22] R.H. Swendsen and J.-S. Wang, Nonuniversal critical dynamics in Monte Carlo simulations, *Phys. Rev. Lett.* **58** (1987) 86.
- [23] U. Wolff, Collective Monte Carlo Updating for Spin Systems, *Phys. Rev. Lett.* **62** (1989) 361.
- [24] C.M. Fortuin and P.W. Kasteleyn, On the random-cluster model: I. Introduction and relation to other models, *Physica* 57 (1972) 536. J.-S. Wang, Clusters in the three-dimensional Ising model with a magnetic field, *Physica A* 161 (1989) 249.
- [25] K. Binder and D.W. Heermann, Monte Carlo Simulations in Statistical Physics, Springer, 1992.
- [26] K. Kanaya and S. Kaya, Critical exponents of a three-dimensional O(4) spin model, *Phys. Rev. D* **51** (1995) 2404.
- [27] J. Engels, L. Fromme and M. Seniuch, Correlation lengths and scaling functions in the three-dimensional O(4) model, *Nucl. Phys. B* **675** (2003) 533.
- [28] M. Oevers, Kritisches Verhalten in O(4)-symmetrischen Spinmodellen und 2-flavour QCD, Diploma thesis, Universität Bielefeld, 1996.
- [29] W. Bietenholz, On the Isomorphic Description of Chiral Symmetry Breaking by Non-Unitary Lie Groups, *Int. J. Mod. Phys. A* 25 (2010) 1699.

- [30] C. Shi et al., Chiral transition and the chiral charge density of the hot and dense QCD matter, J. High Energ. Phys. 06 (2020) 122. A. Ayala et al., Fluctuating temperature and baryon chemical potential in heavy-ion collisions and the position of the critical end point in the effective QCD phase diagram, *Phys. Rev. D* 101 (2020) 074023. Y.P. Zhao, R.R. Zhang, H. Zhang and H.S. Zong, Chiral phase transition from the Dyson-Schwinger equations in a finite spherical volume, *Chin. Phys. C* **43** (2019) 063101. M. Motta *et al.*, Exploration of the phase diagram and the thermodynamic properties of QCD at finite temperature and chemical potential with the PNJL effective model, J. Phys.: Conf. Ser. 1667 (2020) 012029. A. Martínez and A. Raya, An innovative approach for sketching the QCD phase diagram within the NJL model using Lagrange Multipliers, arXiv:1909.12416 [hep-ph]. B.L. Li et al., Finite volume effects on the chiral phase transition from Dyson-Schwinger equations of QCD, Nucl. Phys. B 938 (2019) 298. J. Knaute, R. Yaresko and B. Kämpfer, Holographic QCD phase diagram with critical point from Einstein-Maxwell-dilaton dynamics, *Phys. Lett. B* 778 (2018) 419. J. Goswami et al., Critical end points in (2+1)-flavor QCD with imaginary chemical potential, PoS CORFU2018 (2019) 162. N.G. Antoniou et al., Locating the QCD critical endpoint through finite-size scaling, Phys. Rev. D 97 (2018) 034015. S. Sharma, The QCD Equation of state and critical end-point estimates at $\mathcal{O}(\mu_B^6)$, Nucl. Phys. A 967 (2017) 728. R. Rougemont et al., Dynamical vs. equilibrium properties of the QCD phase transition: a holographic perspective, *Phys. Rev. D* **96** (2017) 014032. P. Kovács and Gy. Wolf, Phase diagram and isentropic curves from the vector meson extended Polyakov quark meson model, Acta Phys. Pol. B Proc. Suppl. 10 (2017) 1107. Z.F. Cui, J.L. Zhang and H.S. Zong, Proper time regularization and the QCD chiral phase transition, Sci. Rep. 7 (2017) 45937. G.A. Contrera, A.G. Grunfeld and D. Blaschke, Supporting the search for the CEP location with nonlocal PNJL models constrained by lattice QCD, Eur. Phys. J. A 52 (2016) 231.
- [31] A. Ayala, S. Hernández-Ortiz and L.A. Hernández, QCD phase diagram from chiral symmetry restoration: analytic approach at high and low temperature using the linear sigma model with quarks, *Rev. Mex. Fis.* **64** (2018) 302.

[32] J.A. García-Hernández, E. López-Contreras, E.N. Polanco-Euán and W. Bietenholz, in preparation.